Research on Engineering Structures & Materials
www.jresm.org
MIM Research Group

Research Article

Prediction of machine learning application in the development of novel sustainable self-compacting geopolymer concrete

Arun B R[1,a], Srishaila J M[2,b], Md Khalid S[*,3,c], Veerabhadrappa Algur[4,d], Kavyashree K[5,e], Tanu HM[3,f]

[1]*Department of Civil Engineering, Dr.AIT, Bangalore, 560072, Karnataka, India*
[2]*Department of Civil Engineering, SJMIT, Chitradurga, 577501, Karnataka, India*
[3]*Department of Civil Engineering, Ballari Institute of Technology and Management, Ballari, 583104, Karnataka, India*
[4]*Department of Mechanical Engineering, RYMCE, Ballari,583104, Karnataka, India*
[5]*Department of Civil Engineering, GPT, Mulbagal, 563131, Karnataka, India*

Article Info

Article History:

Received 16 July 2024
Accepted 21 Nov 2024

Keywords:

Self-compacting geopolymer concrete;
Scanning electron microscope;
Manufactured sand;
Metakaolin;
Ground-granulated blast furnace slag;
Molarity

Abstract

This work conducted experimental research into the flow and mechanical characteristics of self-compacting geopolymer concrete (SCGC) made from ecologically beneficial byproducts of industry such as ground granulated blast furnace slag (GGBFS) and metakaolin (MK). Through trial and error, the mix's proportion of self-compacting geopolymer concrete (SCGC) was determined. The mass fraction of GGBFS with metakaolin was varied by 0%, 10%, 20%, and 30% by mass for all molarities, including 8M, 10M, and 12M. The superplasticizer (S.P.) dose of 1.5% and the fluid-to-binder (F/B) ratio of 0.37 by mass were held constant for each mix percentage, with the extra water content being changed correspondingly. Workability properties were assessed in addition to mechanical properties, which comprised compressive strength, split tensile strength, flexural strength, shear strength, and impact strength. The application of machine learning algorithms to forecast the compressive strength of SCGC is the focus of this study. Specifically, Random Forest (RF), Gradient Boost, and Extreme Gradient Boost (XGB) are utilized. Different success measures, like Root mean squared error (RMSE), mean squared error (MSE), mean absolute error (MAE), and R-squared (R^2), are used to judge these methods. The Gradient Boost model outperforms the others, achieving an R^2 score of 0.934 on training data and 0.929 on test data, showcasing its precision and accuracy. The success of the Gradient Boost model can be attributed to its incorporation of randomness and ensemble diversity, making it a powerful tool for predicting compressive strength in various scenarios.

1. Introduction

The constant winds of change are ever-present in the field of environmental sustainability and design, where carbon dioxide emissions monitoring is used as a comparison metric. The speed with which this change is occurring within our sphere of influence is particularly disturbing. The dominant ideologies that have guided the development of our economy and manufacturing have recently shown signals of extreme unsustain ableness. Our modern world has been shaped in fundamental and widespread ways through the ecological reverberations caused by the unstoppable rise of population and the relentless advance of urbanization. Understanding this

*Corresponding author: khalid.s@bitm.edu.in
[a]orcid.org/0000-0003-3455-8910;[b]orcid.org/0000-0001-6161-9542; [c]orcid.org/0000-0002-4728-099X; [d]orcid.org/0000-0001-6094-6197; [e]orcid.org/0009-0006-0112-3370; [f]orcid.org/0000-0001-9760-9469.
DOI: http://dx.doi.org/10.17515/resm2024.354ma0716rs

complex transition requires analyzing its constituent parts, with due consideration provided to both past data and anticipated future tendencies. Ordinary concrete is a composite miracle in the world of building supplies, consisting of just 12% cement, 8% mixing water, and 80% aggregate. This means that every year, in addition to the astonishing 1.6 billion tons of cement produced worldwide [1], the concrete industry consumes almost 10 billion tons of sand and rock, along with a billion tons of mixing water. The concrete industry is the undisputed giant, using a massive 12.6 billion tons of raw materials every year, making it the world's top natural resource consumer [2]. Cement, the immovable foundation of conventional concrete, is seeing a surge in demand as a result of rising concrete demand. With the unstoppable storm of population growth and the relentless gears of industrialization, the shadow of pollution resulting from cement manufacture grows larger by the year. Unfortunately, cement production is expected to increase from its current 7% of global CO_2 emissions to 17% in the future. At the crossroads of a rapidly expanding sector of construction and a need for environmental stability, a search for harmony begins. Because of this, the cement industry must go beyond its existing narrative, which is centered on increasing cement replacement levels and expanding the use of industrial by-products as SCMs. People are calling for a big change to get rid of cement and instead synthesize new materials that are better for the environment and use less energy [3]. The invention of geopolymer concrete marked a new era in the industry, one that eliminated dealing with the massive fuel costs associated with traditional high-temperature kilns. When compared to the emissions created by one ton of Portland cement, the 0.18 tons of CO_2 produced by the burning of carbon fuel per ton of Geopolymeric cement is a significant improvement. With the development of self-compact geopolymer technology, a novel, non-conventional, cement-free binder has emerged, a wonder that self-compacts without segregation, flowing seamlessly into every corner, undisturbed by obstructive barriers, and embracing formwork with remarkable ease [4].

Metakaolin is widely recognized as a key raw material in the synthesis of geopolymers due to the substantial contributions it makes to our understanding of the material because of the high concentrations of SiO_2 and Al_2O_3 it contains[5]–[7]. In a chemical synergy, calcium hydroxide and metakaolin combine forces to generate hydrated calcium aluminates and silico aluminates, resulting in a significant enhancement of binding strength. Metakaolin boasts an extensive surface area of 12,000 m^2/g, far surpassing that of regular cement [2]. But the fact remains metakaolin's demand places limits on the field of strength creation [8]. When playing with fly ash and GGBFS [9], its high aluminum concentration makes it the silicon-reduction expert. Although cement's demand is unrelenting, it may not be necessary to call for the expansion of current cement plants if available fly ash, GGBFS, and metakaolin are used efficiently [10]. These developments have strengthened the construction industry to the point where it can achieve complete sustainability [11]. And in this complicated web, the investigation's principal aim becomes clear. Still, the primary focus of this study is on the enhancement and functionality of GGBFS-Metakaolin-based self-compacting geopolymer concrete (SCGC). Here, GGBFS plays the role of reference mix, setting the context for the introduction of metakaolin at 0%, 10%, 20%, and 30% of the total mass of GGBFS, respectively. The primary objective of this research is to investigate the relationship between workability and strength, specifically highlighting the complex correlations that arise from the extensive domain of machine learning techniques and compressive strength. A continuous investigation is being conducted to thoroughly examine the complex aspects of microstructural properties, a field that is both mysterious and complicated featuring elaborate structures and intricate patterns.

In the world of materials, scientists like Daniel L.Y. Kong [12] have discovered some interesting connections between different substances, like fly ash and metakaolin, and their strength when exposed to high temperatures. They use special tools to look closely at the materials. They found that fly-ash-based geopolymer materials have tiny pathways that help moisture escape when heated, which keeps the material strong. But metakaolin-based geopolymer materials don't have these pathways and can become weaker. In the present study, Siddique et al.[13] investigate the mysterious phenomenon of water absorption in geopolymer concrete. A complex novel emerges, whereby the amounts of water absorption fluctuate within the mysterious range of 5.8–7.1%. In this context, the central character is the 12M mix, an individual distinguished by its notable

attributes of low water absorption and a substantial volume of permeable voids. The performance shown on the platform of material science demonstrates a profound correlation, whereby the combination of minimal water absorption and permeable void volume results in the emergence of remarkable compressive strength. The author, Jiale Shen et al. [14], discusses machine learning algorithms like gradient boost (GB), random forest (RF), and extreme gradient boost (XGB). Their main interest was in the compressive strength of geopolymers made from building and demolition waste (CDWG). The results are appealing, and the accuracy of the predictions goes beyond $R^2 > 0.9$, striking great heights. Among the maestros, GB and XGB rise to the top, making RF look weak in comparison.

1.1 Research Significance

The novel approach to the study of self-compacting concrete using metakaolin has been extensively carried out and the various machine learning algorithms and strength parameters have been extensively discussed in detail. These new findings point the way toward material optimization and sustainable construction materials. Machine learning in geopolymer concrete is emerging research that will improve the understanding, design, and optimization of geopolymer concrete properties. Geopolymer concrete, a more sustainable alternative to traditional Portland cement concrete, is made using industrial by-products such as slag and metakaolin. Various Machine learning (ML) methods can significantly enhance the performance prediction, mix design optimization, and quality control of this material. The new things that have been conducted in this current research are the prediction of experimental results with random forest, gradient boost, extreme gradient boost, evaluation, mean absolute error, mean square error, root mean square error, and R Square.

2. Materials

The binder materials employed in the experimental work are GGBFS and Metakaolin. GGBFS is rich in calcium oxide whereas metakaolin is rich in alumina & silica. Hence the use of these two binders will result in long strength gain and early-stage reactivity ensuring balanced strength development. Other materials like fly ash, Rice husk ash, and sugarcane bagasse ash can also be used, but GGBS and Metakaolin show higher reactivity, especially in cold conditions, where fly ash and other binders can take longer to react. Concrete with GGBS & metakaolin tends to have low thermal shrinkage and creep compared to other materials. This property is essential for large-scale construction.

2.1. Ground-Granulated Blast Furnace Slag (GGBFS)

Silica and calcium oxide make up GGBFS, a granular, non-metallic substance crushed to less than 45 microns [15]. The physical and chemical characteristics of GGBS are shown in Table 1. The chemical composition test results of GGBFS are in accordance with the specifications.

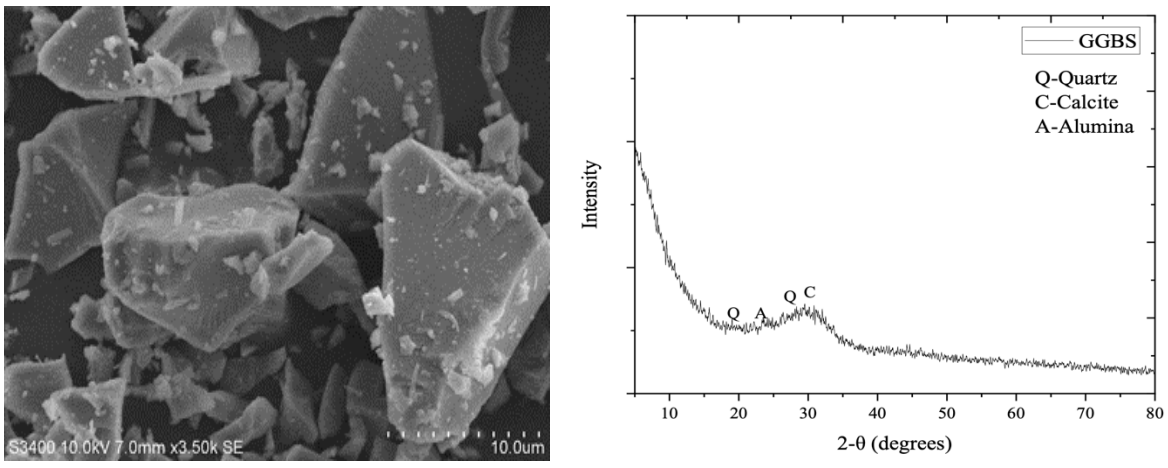

(a) (b)

Fig. 1. (a) SEM image of GGBFS; (b) XRD Diffraction patterns of GGBFS

The morphology of the GGBFS SEM micrographs Fig 1 (a) is approximately angular, brittle, and elongated. The GGBFS XRD reveals the presence of a notable amorphous phase composed of alumina, calcite, and quartz Fig 1 (b). From Fig.1(a) SEM image it is noticed that the GGBS material is angular in shape with irregularly shaped particles present in it.

3.2. Metakaolin

Metakaolin is a pure, amorphous, extremely reactive pozzolana aluminium silicate that forms stable hydrates with lime in water and gives mortar hydraulic characteristics. The physical and chemical characteristics of Metakaolin are in Table 1. Powder-based Metakaolin Fig 2 (a) SEM micrographs are amorphous. Metakaolin XRD Fig 2 (b) reveals MK humps and peaks from 20° to 35°, indicating an amorphous phase with quartz, mullite, muscovite, and anatase peaks. From Fig.2(a) SEM image, it is seen that metakaolin shows platy in nature.

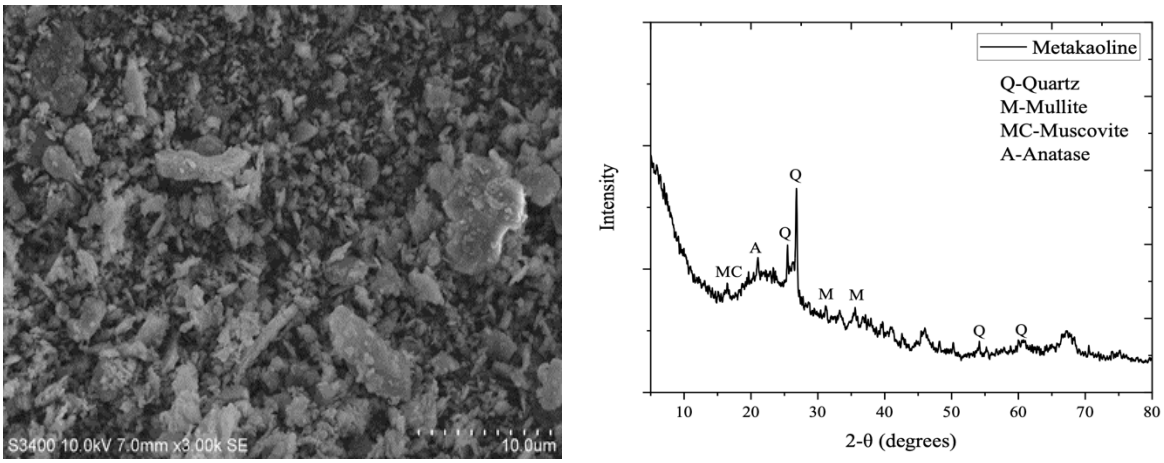

(a) (b)

Fig. 2. (a) SEM image of metakaolin; (b) XRD diffraction of metakaolin

Table 1. Physical and chemical properties of GGBFS and metakaolin

Parameters	GGBFS	Metakaolin
	Physical Properties	
Colour	Light grey	White
Specific Gravity	2.7	2.01
Surface Area	450 m^2/kg	1200 m^2/kg
	Chemical Properties	
SiO_2	33.77%	52%
CaO	33.77%	---
Al_2O_3	13.24%	42.2%
MgO	8.46%	---
Fe_2O_3	0.05%	0.7%
Mno	0.65%	---
Sulphide Sulphur	2.23%	---
Total chlorides	0.01%	---

2.3. Alkaline Activators Preparation

This study employed an alkaline solution of NaOH and Na_2SiO_3. Sodium silicate aids in binder dissolution. Sodium hydroxide pellets in water create a solution at the right concentration. The molar content of sodium hydroxide solution varies. Before mixing with sodium silicate, this solution undergoes treatment for 24 hours. After mixing, the polymerization process reacts and produces heat, so leave it for 20 minutes before using. The entire research used a ratio of sodium silicate solution to sodium hydroxide is 2.5. Sodium hydroxide pellets have 99% purity and 2.13 specific gravity. The Sodium silicate consists of 14.43% Na_2O, 29.55% of SiO_2, 56.11% of water with 74 Pa.sec viscosity specific gravity of 1.55 and pH is 12.

2.4. Super Plasticizer (S.P)

Master Glenium SKY 823 has a pH of >6, a relative density of 1.08 + 0.01 at 250 °C, and a chloride ion concentration of <0.2%.

2.5. Aggregates

Using M-SAND as a fine aggregate, this study found 2.59 specific gravity, 2.2% water absorption, and grade "Zone II". The coarse aggregate employed in this study has 2.67 specific gravity, 0.65% water absorption, 15.23% combination index, and 28.98% crushing value. The test sample meets IS: 383-2011 standard [16].

2.6. Mix Proportions

In the current study, metakaolin was employed to substitute twelve GGBFS blends at mass proportions of 0%, 10%, 20%, and 30% with 8M,10M, and 12M of sodium hydroxide solution. For SCGC workability, the superplasticizer was held at 12% for all molarities and the binder was adjusted with extra water according to molarities by mass to gain the required workability of SCGC. Table 2 shows the GGBS/metakaolin-based SCGC Mix Proportion details

Table 2. Mix proportion of GGBFS/Metakaolin-based SCGC

Mixes	Binder Components (%)	GGBFS (Kg/m^3)	Metakaolin (Kg/m^3)	M-Sand (Kg/m^3)	Coarse Aggregate (Kg/m^3)	NaOH+ water (Kg/m^3)	Na_2SiO_3 (Kg/m^3)	Molarity (M)	Extra Water (%)
M1	GGBFS 100% & MK 0%	434.68	0	695	1044	64.75	161.875	8M	6
M2	GGBFS 90% & MK 10%	391.21	43.47	695	1044	64.75	161.875	8M	8
M3	GGBFS 80% & MK 20%	347.74	86.94	695	1044	64.75	161.875	8M	10.5
M4	GGBFS 70% & MK 30%	304.28	130.4	695	1044	64.75	161.875	8M	12.5
M5	GGBFS 100% & MK 0%	434.68	0	695	1044	66.18	165.45	10M	6.5
M6	GGBFS 90% & MK 10%	391.21	43.47	695	1044	66.18	165.45	10M	9
M7	GGBFS 80% & MK 20%	347.74	86.94	695	1044	66.18	165.45	10M	11
M8	GGBFS 70% & MK 30%	304.28	130.4	695	1044	66.18	165.45	10M	13
M9	GGBFS 100% & MK 0%	434.68	0	695	1044	67.5	168.77	12M	7
M10	GGBFS 90% & MK 10%	391.21	43.47	695	1044	67.5	168.77	12M	10.5
M11	GGBFS 80% & MK 20%	347.74	86.94	695	1044	67.5	168.77	12M	12
M12	GGBFS 70% & MK 30%	304.28	130.4	695	1044	67.5	168.77	12M	14

2.7. Preparation of Concrete, Casting/Curing

Before making the new SCGC, GGBFS, metakaolin, and manufactured sand were blended in the right amounts. The coarse aggregate was then added to the mixer in a specific proportion in a saturated dry surface (SSD) state and mechanically mixed for 2.5 min. After the dry mix, a well-shacked liquid combination (F/B) with the alkaline solution, superplasticizer, and additional water was pumped into the mixer for at least 3 minutes to combine it. Extra water has been added to the mix based on trial and error to maintain the flowability of the developed self-compacting geopolymer concrete. The addition of extra water was necessary to achieve the desired workability of the self-compacting geopolymer concrete. Without sufficient water, the concrete would have been too dry and difficult to work with. The freshly formed concrete was evaluated for significant working characteristics to categorize self-compacting concrete. Also,

slump flow, V-funnel, and L-box tests were assessed for workability properties. Hardened properties for specimens were produced following new SCGC testing. After vigorous hand mixing, the new concrete was poured into moulds without compaction into cubes, cylinders, prisms, etc., filling all moulds spaces with their weight. Scraping the specimens top removed surplus material and flattened them. Three samples were cast and evaluated for each combination in the experiment. After casting, samples, and moulds were oven-baked at 700 °C for 24 hours. After this oven-drying cycle, the study samples were taken from the moulds and kept at room temperature until test day.

3. Fresh Properties and Test Results of SCGC

The fresh characteristics of SCGC mixes were assessed using three SCC parameters according to EFNARC guidelines [16]. They are filling, passing, and segregation resistance. The current research assessed these features for all molarities utilizing Slump Flow, V-Funnel, and L-Box. Table 3 displays the workability test results.

Table 3. Workability test results for SCGC

Mixes	M1	M2	M3	M4	M5	M6	M7	M8	M9	M10	M11	M12	Range of workability values for SCC
Slump Flow (mm)	685	660	655	655	675	655	650	640	660	650	650	635	650-800 mm
V-Funnel (sec)	10.9	11.5	12	13	11	12	12.5	13.5	12	12.21	13	14	6-12 Sec
L-Box (H2/H1)	0.89	0.85	0.84	0.82	0.87	0.83	0.83	0.82	0.85	0.82	0.8	0.79	0.8-1.0

As shown in Fig 1 (a), GGBFS particles are flaky and elongated and have a large surface area, while metakaolin particles are amorphous and have a large surface area (Fig 2 (a) and Table 1), making it difficult to achieve the EFNARC-required flow. The slump flow is lowered for 10%,20%and 30% metakaolin replacement by 3.6% to 4.3%, 2.9% to 5.1%, and 1.5% to 3.7% compared to the control mix (GGBFS 100) for 8M, 10M, and 12M. Slump flow percentage decreases by 3.6% for reference mix M1 from 8M to 12M, 1.5%, 0.7%, and 3.05% for mixes M2, M3, and M4. The V-funnel test evaluates the filling capability of SCGC, showing an increase in flow time with metakaolin percentage. At 12M, all values slightly exceeded the specified limit. Substituting 10%,20% and 30% metakaolin for the control mix increases V-funnel flow time by 5.5% to 19.26%, 9% to 22.72%, and 1.75% to 16.66%, respectively.

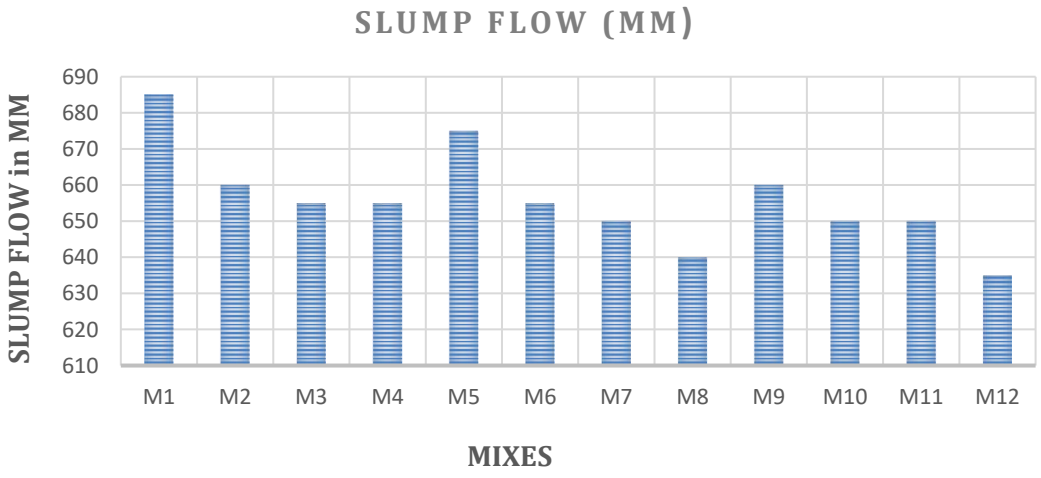

Fig. 3. Slump flow value for all the mixes

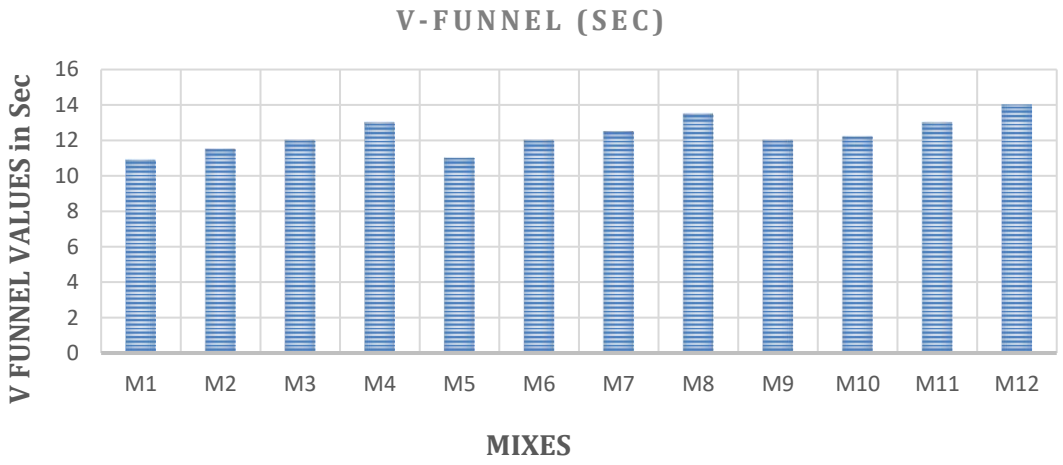

Fig 4. V Funnel value for all the mixes

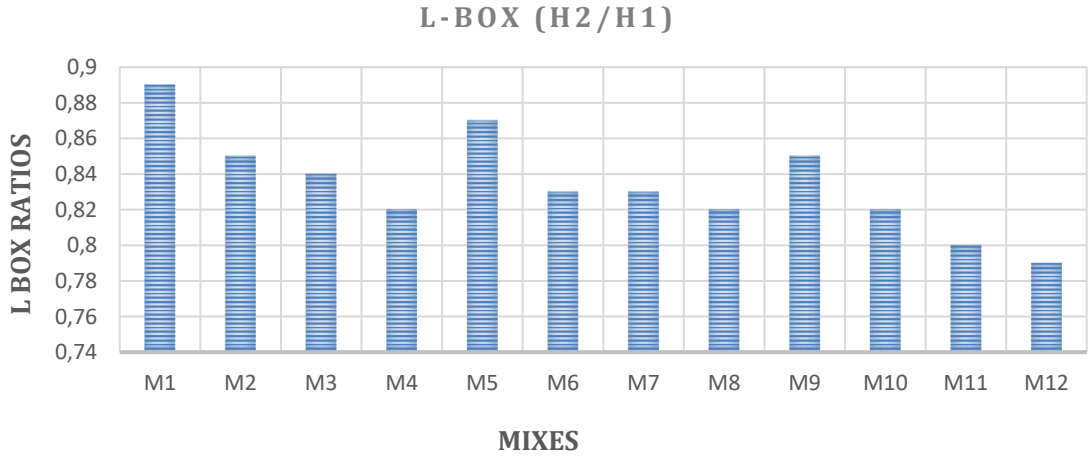

Fig 5. L Box ratios for all the mixes

The V-funnel flow time for reference mix M1 increased by 10% from 8M to 12M, while for mixes M2, M3, and M4, it increased by 6.17%, 8.33%, and 7.7%, respectively. The blocking ratio of L-box decreases with increased metakaolin content and sodium hydroxide concentration, similar to slump flow and V-Funnel test results. However, replacements of metakaolin with 10%, 20%, and 30% decrease the blocking ratio by 4.50% to 7.86%, 4.6% to 5.7%, and 3.5% to 7.0%, respectively. The percentage decrease from 8M to 12M for replacing GGBFS with metakaolin by 0%, 10%, 20%, and 30% is 4.5%, 3.52%, 4.76%, and 3.65%, respectively.

4. Hardened Properties of Self-Compacting Geopolymer Concrete

4.1. Compressive Strength Tests

This experiment evaluated the compressive strength of a cube sample 100mm in a digital 2000KN compression testing machine (CTM) following IS 516-1959 [17] guidelines. The study found that increasing the percentage of metakaolin in the sample resulted in a decrease in strength. However, as the molarity increased, the strength also increased [3].

The percentage decrease in strength by replacing GGBFS with 10%, 20%, and 30% of metakaolin when compared to the control mix GGBFS 100 at the end of 90 days was around 2.10% 4.21% 12.63% for 8M, 7.54%,11.32%,16.03% for 10M and 8.20%,11.47%,6.40% for 12M of sodium hydroxide solution. The percentage increase in strength from 8M to 10M and from 10M to 12M at the end of 90days was 11.57% and 15.09% for the M1 series, 5.37% and 14.28% for the M2 series, 3.23% and 14.89% for the M3 series, and 9.87% and 14.60% for the M4 series. Table 4 shows compressive strength test results and Fig 6 shows compressive strength values for various mixes.

Table 4. Compressive strength test results in MPa

Mix Id	3 days	7 days	28 days	56 days	90 days	Molarity
M1	41	42	45	46	47.5	8
M2	40.5	41.5	44	45	46.5	
M3	39	40	42.5	44	45.5	
M4	38	38.5	40	40.5	41.5	
M5	46	47.5	50	51.5	53	10
M6	43	44	47	47.5	49	
M7	41.5	42	44.5	46	47	
M8	40	41	43	44	44.5	
M9	49	50	56.5	59	61	12
M10	47.5	48	53.5	55	56	
M11	45	46	52	53	54	
M12	44	44.5	49	50	51	

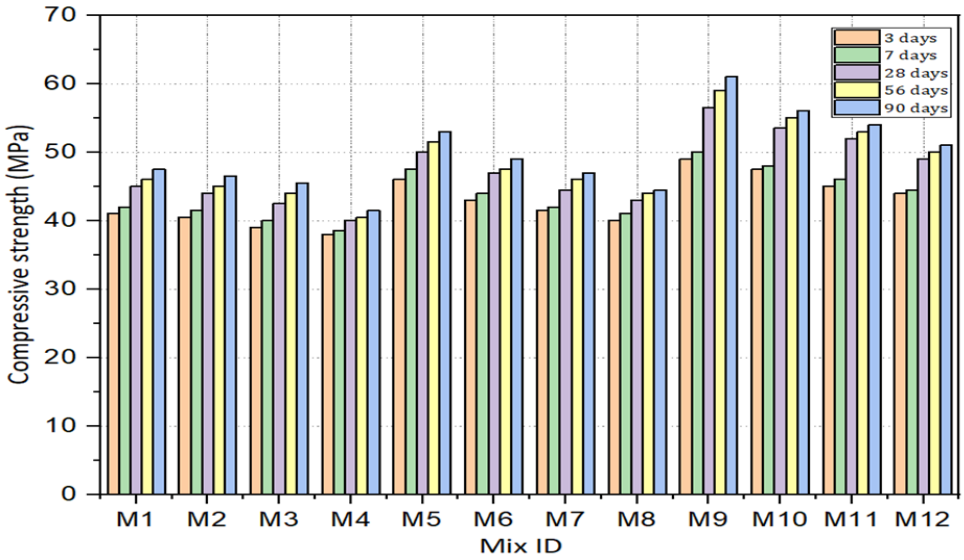

Fig 6. Compressive strength test results

4.2. Split Tensile Strength Tests

The experiment was conducted in a CTM on a 150 mm diameter and 300 mm height cylinder specimen according to IS 516-1959 [17]. The tensile strength decreased with increased metakaolin content and increased with increased molarity compared to the control mix.

Table 5. split strength test results in MPa

Mix Id	7 Days	28 Days	56 Days	Molarity
M1	4.25	4.67	4.73	8
M2	3.96	4.2	4.38	
M3	3.82	3.96	4.1	
M4	3.53	3.67	3.82	
M5	4.7	4.85	5	10
M6	4.37	4.5	4.9	
M7	4.2	4.35	4.5	
M8	3.9	4.2	4.25	
M9	5.2	5.5	5.55	12
M10	4.8	4.95	4.98	
M11	4.6	4.7	4.74	
M12	4.3	4.5	4.63	

The percentage decrease in strength by replacing GGBFS with 10%, 20%, and 30 % of metakaolin when compared to the control mix GGBFS 100 at the end of 56 days was around 7.39%, 13.32%,19.23% for 8M, 2%,10%,7.64% for 10M and 10.27%,17.08%,19.87% for 12M. After 56 days, the M1 series increased by 5.70% and 11% from 8M to 10M and 10M to 12M, the M2 series by 11.87% and 1.63%, the M3 series 9.75% and 5.33%, and the M4 series 8.94%. Table 5 shows split strength test results and Fig 7 shows split tensile strength values for various mixes.

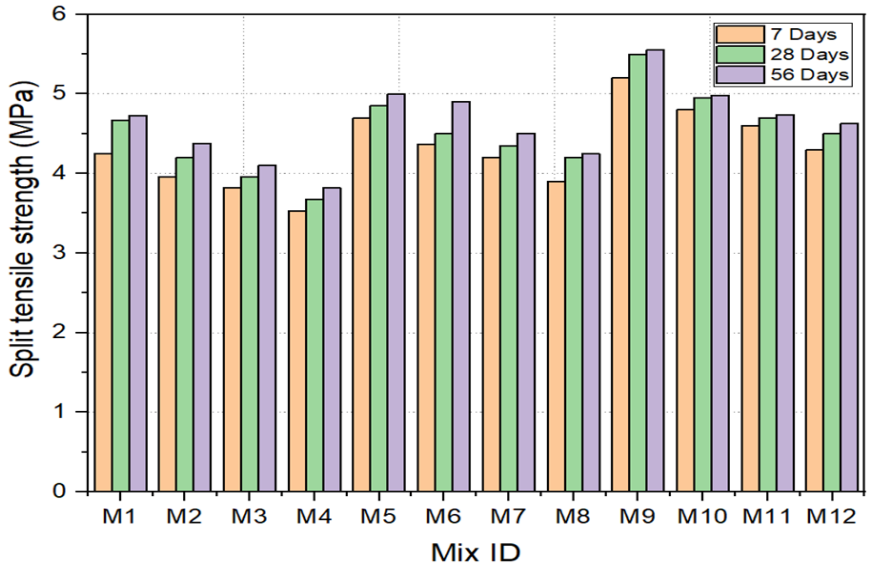

Fig 7. Split tensile strength test results

4.3. Flexural Strength Tests

The 100×100×500 mm sample was tested in a flexural testing machine. Increasing metakaolin concentration lowers flexural strength, whereas increases with greater molarity. At 56 days, the percentage drop in strength for 10%,20% & 30% replacement of GGBFS when compared to control mix GGBFS100 was around 1.65%,2.68%,6.40% for 8M, 1.1%,3%,4% for 10M and 19.20%, 22.24%,21.28% for 12.

Table 6. Flexural strength test results in MPa

Mix Id	7 Days	28 Days	56 Days	Molarity
M1	4.62	4.68	4.85	8
M2	4.57	4.59	4.77	
M3	4.51	4.65	4.72	
M4	4.37	4.49	4.54	
M5	4.35	4.92	5	10
M6	4.7	4.85	4.95	
M7	4.61	4.77	4.85	
M8	4.4	4.72	4.8	
M9	5.1	5.45	6.25	12
M10	4.82	4.92	5.05	
M11	4.75	4.81	4.86	
M12	4.6	4.72	4.92	

M1 series strength increases from 8M to 10M and 10M to 12M at 56 days are 3.09% and 25%, M2 series is 3.77% and 2.02%, M3 series is 2.75% and 0.2%, and M4 series is 5.72% and 2.5%. Table 6 shows flexural strength test results and Fig 8 shows flexural strength values for various mixes.

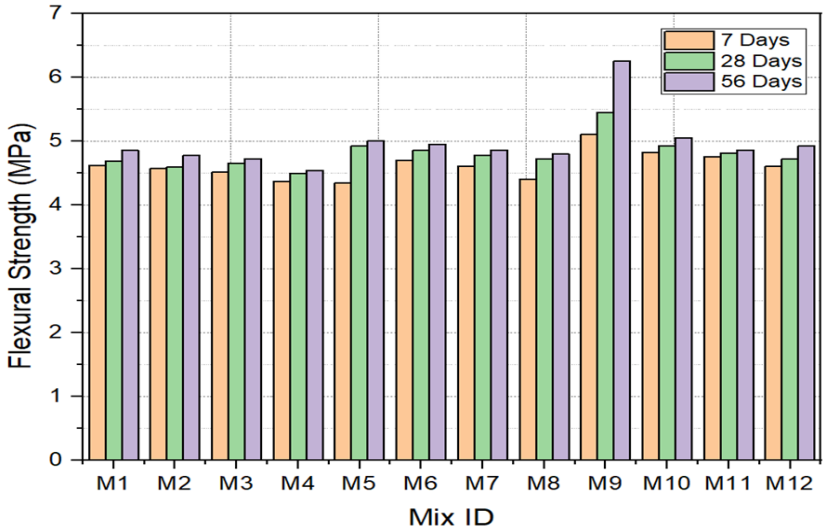

Fig 8. Flexural strength test results

4.4. Shear Strength Tests

Bairagi and Modhera [18] and Baruah and Talukdar [19] recommended applying shear strength tests on an L-shaped shear test specimen on self-compacting geopolymer concrete in the absence of a code. Inserting a 90× 60 ×150 mm steel block into 150 mm side-cube moulds before pouring concrete generated the samples. Shear test specimen details are in Fig 9. In a CTM system, the sample was loaded till failure.

Fig. 9. Details of the shear test

Table 7. Shear strength test results in MPa

Mix Id	7 Days	28 Days	56 Days	Molarity
M1	4.44	4.6	4.65	8
M2	3.89	4.05	4.15	
M3	3.22	3.35	3.47	
M4	2.95	3	3.1	
M5	4.5	4.65	4.7	10
M6	3.97	4.1	4.2	
M7	3.28	3.4	3.51	
M8	3.02	3.07	3.14	
M9	4.62	4.7	4.74	12
M10	4.2	4.25	4.3	
M11	3.35	3.43	3.54	
M12	3.1	3.15	3.2	

Replacement of GGBFS with metakaolin for 8M, 10M, and 12M lowers strength by 10.75,25.37%, and 33.33% for 8M,10.63%,25.31% and 33.19% for 10M, and 9.28%,25.31% and 32.48% for 12M compared to control mix M1(GGBFS100) after 90 days. The M1 series has a 1.07% and 0.85% strength increase from 8M to 10M and 10M to 12M after 90 days, whereas the M2 series has 1.20% and 2.38%, the M3 series 1.15% and 0.85%, and the M4 series 1.29% and 1.91%. IS 456-2000 [20] suggests M20 grade (conventional) concrete has a maximum shear strength of 2.5 MPa. Regardless of molarity, all mixtures, including the reference mix, exceeded 2. 5MPa.In recent studies, it was also observed that geopolymer concrete gave remarkable and positive results for bonding and interface [27]. Table 7 shows shear strength test results and Fig 10 shows shear strength values for various mixes.

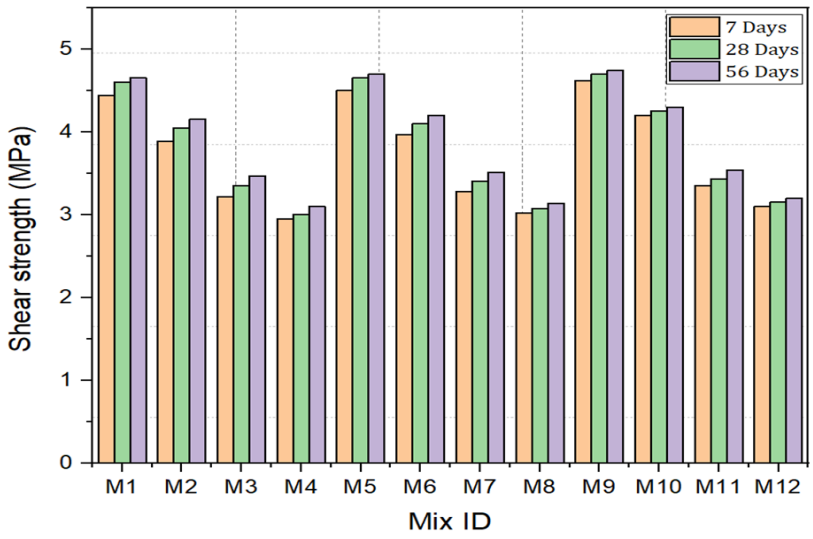

Fig. 10. Shear strength test results

4.5. Impact Strength

Self-compacting geopolymer concrete impact strengths were measured using Schruder's impact test equipment. This is exactly 150 mm-diameter, 60 mm-thick samples were selected. Fig 11 (a) & (b) show a 45.4 N hammer (ball) from 457 mm being lowered in Schruder's impact evaluation system. Observe the number of blows needed for the first and final breakdown. The final crack indicates that the specimen has structurally failed under the impact loads. Cracks in the sample sufficiently under impact loads at least three of four concrete portions on the base plate are the ultimate failure.

(a) (b)

Fig 11. (a) Impact test setup; (b) failure of impact specimen

Table 8. Impact Energy of GGBS/Metakaolin-based SCGC

Mix	Molarity	28 Days		56 Days		90Days	
		First crack	Final crack	First crack	Final crack	First crack	Final crack
M1	8M	1515	1597	1618	1722	1743	1805
M2		1452	1494	1514	1556	1597	1639
M3		1348	1411	1411	1452	1514	1556
M4		1183	1245	1245	1286	1328	1390
M5	10M	1618	1701	1763	1846	1867	1950
M6		1556	1639	1618	1680	1701	1763
M7		1494	1577	1556	1618	1639	1722
M8		1411	1514	1473	1535	1514	1556
M9	12M	1660	1763	1888	1950	2012	2157
M10		1597	1660	1701	1763	1805	1867
M11		1535	1597	1618	1680	1701	1763
M12		1452	1514	1535	1597	1618	1680

Based on ACI Committee 544's [21] procedure, Table 8 displays specimen impact strengths and ultimate failure. GGBFS is replaced with metakaolin for 10%, 20%, and 30% and evaluated for all molarities at 28, 56, and 90 days. As the metakaolin content increases, compressive strength increases but the impact resistance decreases. This is due to the denser, more brittle matrix formed by the metakaolin, which reduces the material's ability to absorb and distribute impact energy, leading to cracks under impact loads. The energy absorption capacity of SCGC increased with molarity regardless of the mix, and a 10% substitution of GGBFS with metakaolin improved energy absorption for all testing days. The percentage improvement in strength at ultimate failure from 8M to 10M and 10M to 12M with 10% metakaolin substitution of GGBFS at 90 days is 7.56% and 5.89%.

5. Microstructure Studies

The SEM images from Fig 12 (a)-(b) & (e) -(f) for 8 molarity and Fig 12 (c)-(d) & (g) – (h) for 12 molarity of hardened geopolymer concrete samples after 3 days and 28 days compressive strength tests made with GGBFS100 mix (GGBFS100%) and GM70 mix (GGBFS 70% and metakaolin 30%) demonstrate binder composition and molarity microstructure. Early-stage hydration of calcium aluminates produces needle-shaped prismatic crystals referred to as Ettringite [Fig. 12 (a)]. At 28 days, this Ettringite vanished and became a solid concrete structure [Fig. 12(b)]. All SEM image of SCGC having 12 M of Na (OH) solution show a thick GGBFS composite microstructure with slag grains and few microfractures. High-pozzolanic GGBFS particles produce a denser matrix, resulting in better strength after 28 days. GGBFS composite SEM images (b), (d), (f), and (h) reveal good matrix-GGBFS particle interfacial bonding at 28 days. GGBFS substituted with metakaolin did not show Ettringite. The SEM images from (e) to (h) indicate a strong, compact microstructure as metakaolin expanded due to its huge surface area. As seen in SEM images (e) and (f), metakaolin concentration increases in C-S-H crystals after 3 days. Higher curing times diminish C-S-H crystals by increasing their strength. Due to the large surface area of GGBFS and metakaolin, extra water was provided to ensure flow, resulting in the increase of small pores and micro-cracks as seen in SEM images from (e) and (h), which may explain the decrease in strength with increased metakaolin content. Higher amounts of NaOH break up metakaolinite particles and make the bond between monomers more reactive, which makes the geopolymer's intermolecular bonding stronger. SEM images (c), (d), (g), and (h) of SCGC having 12 M of Na (OH) solution have a more compact and denser microstructure than (a), (b), (e), and (f). Samuel Demie et al. [22] used a field emission scanning microscope (FESEM) to analyze SP dosage. They found dense ITZ development between aggregate and binder matrix at high SP dosages and vice versa, resulting in high compressive strength.

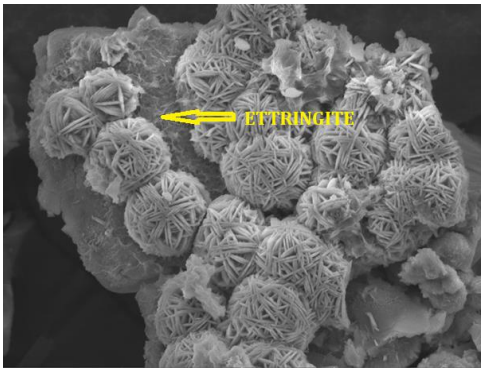

(a) GGBFS100 for 3 days (8M)

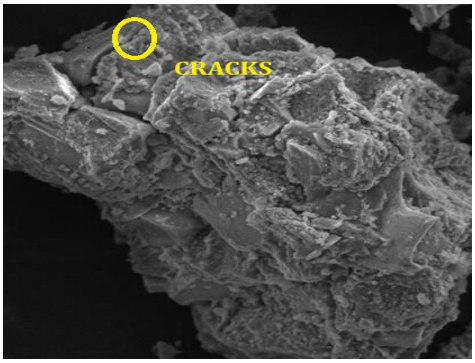

(b) GGBFS100 for 28 days (8M)

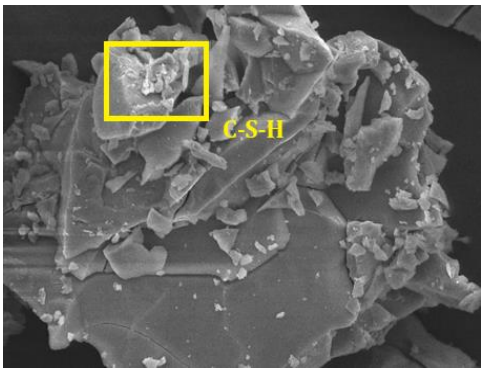

(c) GGBFS100 for 3 days (12M)

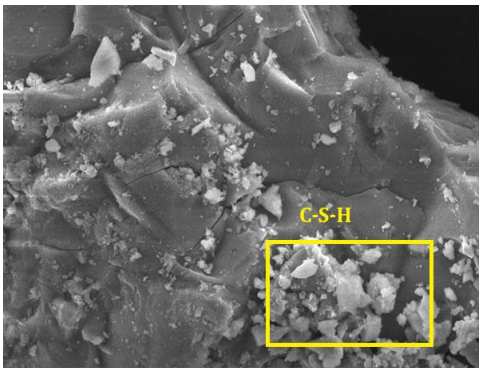

(d) GGBFS100 for 28 days (12M)

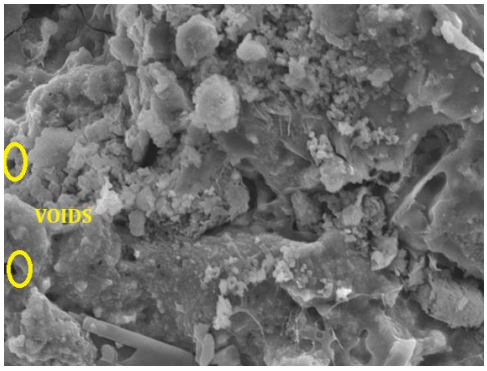

(e) GGBFS70+MK30 for 3 days (8M)

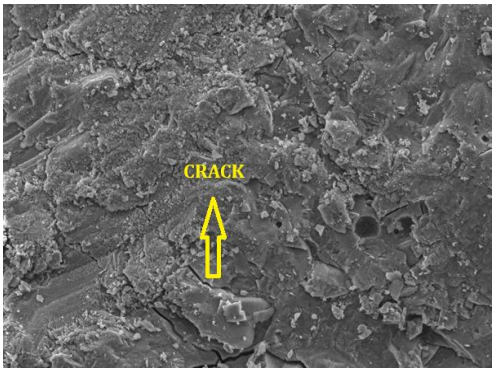

(f) GGBFS70+MK30 for 28 days

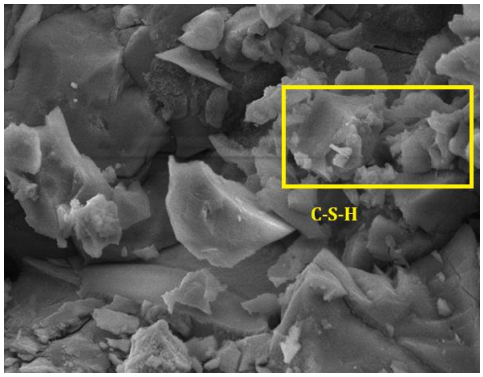

(g) GGBFS70+MK30 for 3 days

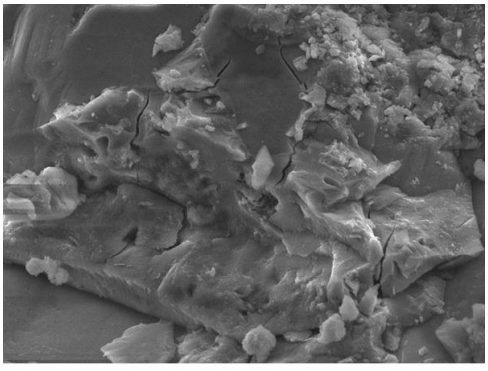

h) GGBFS70+MK30 for 28Days

Fig. 12. SEM images of GGBFS/Metakaolin based SCGC w.r.t Different binder composition and molarity

6. Application of Machine Learning (ML) Methods

6.1 Random Forest

The Random Forest Regressor is a potent machine-learning algorithm employed for regression tasks. Its core mechanism involves the amalgamation of multiple decision trees to improve the robustness and accuracy of predictions. Each decision tree taught by a Random Forest (RF) Regressor uses a unique, randomly selected section of the training data, some of which may be repeated. This procedure is commonly referred to as bootstrap aggregating or bagging. The amalgamation of these decision trees through ensemble averaging serves the dual purpose of introducing randomness and mitigating overfitting, ultimately resulting in reduced variance and an overall improvement in the model's predictive accuracy [23]. The algorithm is mentioned below.

Training data D = $\{(x_i, y_i)\}_{i=1}^{n}$, number of trees T, number of features m to randomly select to each split.

1. For each tree t (from 1 to T)

- Randomly sample n data points from D with replacement (bootstrapping).
- Use the bootstrapped dataset to train the t-th decision tree.
- At each split in the tree:
  - Randomly select mmm features from the total features.
  - Find the best split using one of the selected features.
- Grow the tree until a stopping condition is met (e.g., max depth, minimum samples per leaf).

2. Store the trained decision tree $f_t(x)$

3. Prediction

If there are T decision trees in the forest, the prediction $\hat{y}$ For a new input x is the average of the predictions from all trees:

$$\hat{y} = \frac{1}{T}\sum_{t=1}^{T} f_t(x) \tag{1}$$

Where; T is the total number of trees, $f_t(x)$ is the prediction from the t-th tree for input x.

6.2 Gradient Boost

Gradient Boosting is an ensemble machine learning technique that builds predictive models by merging multiple weak learners, typically decision trees, sequentially. It begins with a simple model and progressively adds more trees, each designed to correct the errors of the preceding ones. Gradient Boosting minimizes the loss function gradient, adjusting model parameters to improve predictions. It's highly effective for regression and classification tasks, providing robust and accurate results. Regularization techniques like learning rate control the overfitting [24]. The formula for the calculation of the predicted values and the residual errors at each iteration is mentioned below: Predicted Value (F) at iteration m:

$$F_m(x) = F_{(m-1)}(x) + learning\ rate * h_m(x) \tag{2}$$

$F_m(x)$ represents the predicted value after adding the m-th tree. $F_{\{m-1\}}(x)$ represents the anticipated or projected value derived from the preceding iteration. learning rate is a hyperparameter that quantifies the individual tree contributions (usually < 1). $h_m(x)$ is the prediction made by the m-th decision tree. Residual Error (R) at iteration m:

$$R_m(x) = y - F_m(x) \tag{3}$$

$R_m(x)$ represents the residual error, which is the key distinction between the actual target value (y) and the predicted value at the m-th iteration ($F_m(x)$).

6.3 Extreme Gradient Boost

XGB is a well-known machine learning ensemble algorithm known for its exceptional performance in regression and classification tasks. It enhances the traditional gradient boosting technique by incorporating regularization, parallel processing, and handling missing data effectively. XGB constructs a set of decision trees in an iterative fashion, optimizing them to minimize a defined loss function. It employs gradient descent and a second-order gradient for faster convergence. The algorithm's distinctive features include pruning to prevent overfitting and automatic handling of missing values [24]. The algorithm is mentioned below. Training data $D = \{(x_i, y_i)\}_{i=1}^{n}$, number of boosting rounts T, learning rate η, loss function $l(y, \hat{y})$, regularization parameters γ and λ.

1. Initialize the model:

- Set initial predictions $\hat{y}_i{}^0$= mean (y)

2. For each boosting round t (from 1 to T)

- Compute residuals for each observation:

$$r^t{}_i = -\frac{\partial l(y_i - \hat{y}_i{}^{t-1})}{\partial \hat{y}_i{}^{t-1}} \tag{4}$$

- Train a decision tree $f_t(x)$ to fit the residuals $r_i{}^t$
- Calculate the leaf weights $w_j$for the tree $f_t(x)$ using:

$$w_j = -\frac{\sum_{i\epsilon leaf\ j} r_i^t}{\sum_{i\epsilon leaf\ j} h_i^t + \lambda} \tag{5}$$

- Where h_i^t is the second derivative of the loss function. Update predictions:

$$\hat{y}_i^t = \hat{y}_i^{t-1} + \eta f_t(x_i) \tag{6}$$

3. Add regularization term:

$$\mathcal{L} = \sum_{i=1}^{n} l\left(y_i \hat{y}_i{}^t\right) + \sum_{k=1}^{t} \gamma\left(f_k\right) \tag{7}$$

For a given dataset with n observations, the objective function $\mathcal{L}$ to be minimized is:

$$\mathcal{L} = \sum_{i=1}^{n} l\left(y_i \hat{y}_i{}^t\right) + \sum_{k=1}^{t} \mathcal{L}\left(f_k\right) \tag{8}$$

Where; $l\left(y_i \hat{y}_i{}^t\right)$is the loss function, typically Mean Squared Error for regression;

$$l\left(y_i \hat{y}_i{}^t\right) = \left(y_i - \hat{y}_i{}^t\right)^2 \tag{9}$$

$\mathcal{L}(f_k))$ is the regularization term that penalizes the complexity of each tree, f_k defined as;

$$\mathcal{L}(f_k) = \Upsilon T + \frac{1}{2}\lambda \sum_{j=1}^{T} w_j{}^2 \tag{10}$$

Where; T is the number of leaves in the tree, W_j represents the weight of leaf j.

6.4 Evaluation

The evaluation of regression models in machine learning encompasses the use of many measures to assess their performance in predicting continuous numeric values. In this work, we have used four evaluative metrics namely, Mean Absolute Error (MAE), Mean Squared Error (MSE), Root Mean Squared Error (RMSE), R-squared (R^2) Score [23].

6.4.1 Mean Absolute Error (MAE)

The Mean Absolute Error (MAE) is a metric that quantifies the average absolute difference between the anticipated values and the actual target values. It provides a straightforward understanding of prediction errors [21].

$$MAE = \left(\frac{1}{n}\sum(predicted - actual)\right) \tag{11}$$

6.4.2 Mean Squared Error (MSE)

MSE calculates the average squared difference between predicted and actual values. It amplifies the impact of larger errors and is widely used in regression evaluations.

$$MSE = \left(\frac{1}{n}\right)\left(\sum(predicted - actual)^2\right) \tag{12}$$

6.4.3 Root Mean Squared Error (RMSE)

RMSE provides an interpretable metric in the same units as the target variable and is calculated as the square root of MSE. Large errors are penalized more severely than MAE.

$$RMSE = \sqrt{MSE} \tag{13}$$

6.2.4 R-squared (R^2) Score

R^2 measures the proportion of the dispersion in the target variable that is predictable from the independent variables. It ranges from 0 to 1, where 1 indicates a perfect fit and 0 implies that the model doesn't explain any variance [25].

$$R^2 = 1 - \left(\frac{MSE(model)}{MSE(mean)}\right) \tag{14}$$

7. Results and Discussion

In this work, the ML models are implemented on the experimental dataset to predict the compressive strength. Implementing ML models using optimization strategies improves accuracy [26,28]. Table 9 lists hyperparameters and evaluation matrix findings.

Table 9: Optimization parameters and performance of ML algorithms

ML Model	R^2 training	R^2 test	MAE	MSE	RMSE	Optimized parameters
RF	0.909	0.822	1.122	2.486	1.576	n_estimator=100
XGB	0.935	0.845	0.575	1.851	1.360	Random state=42
GB	0.934	0.929	0.593	1.852	1.361	Learning rate=0.35

The optimized parameter(n_estimator=100) involves generating 100 independent trees, contributing to improving the prediction accuracy. A higher value generally enhances the performances of models. Random state 42 ensures reproducibility, and learning rate=0.35 controls step size, balancing model accuracy, and overfitting. Cross-fold validation is utilized with value K=10 for all the ML models as another optimization approach. The results of the individual models are discussed in detail below:

7.2 Random Forest

Fig 13 (a) depicts the correlation seen between the experimental values and the predicted values obtained from the RF model. The scatter plot visually represents the training data with red data points and the test data with blue data points. The solid black line represents the optimal fit of the model, while the red and blue dotted lines represent the training and test datasets,

respectively. The RF model was implemented, yielding an R^2 score of 0.909 on training data and 0.822 on test data.

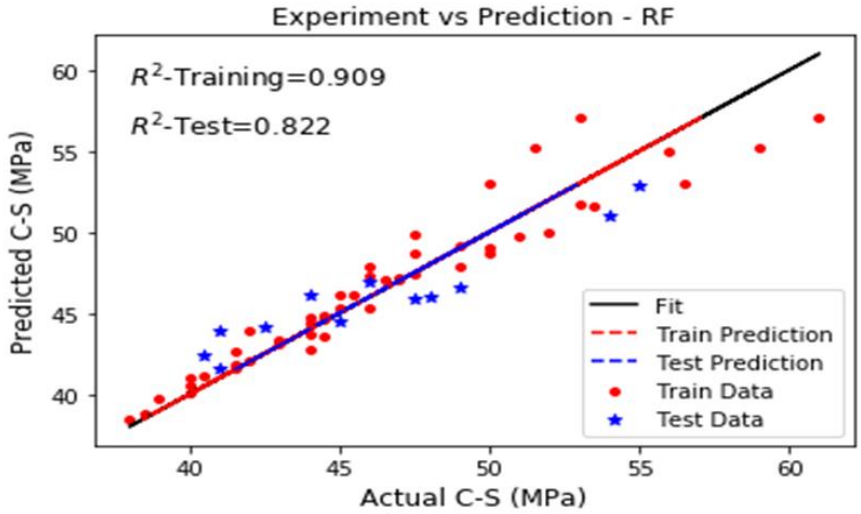

(a)

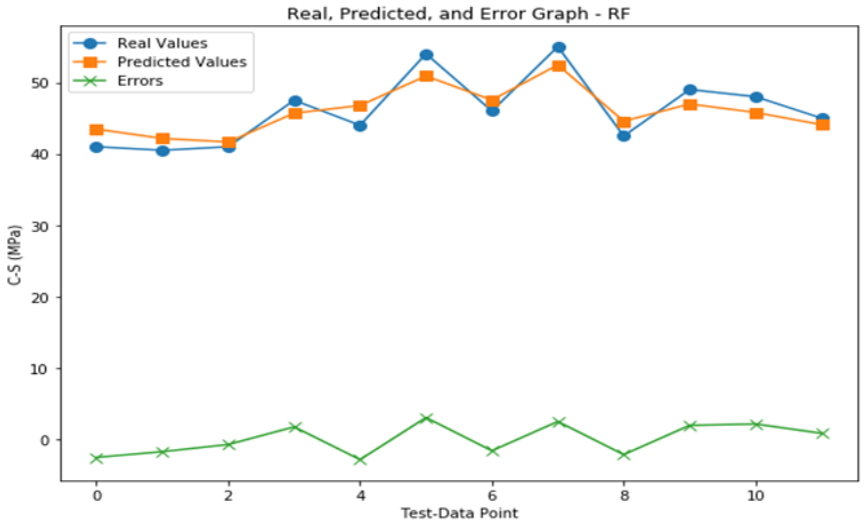

(b)

Fig. 13. (a) Correlation between the actual and predicted RF model results and b) Error graph- RF

Fig 13 (b) illustrates a similarity between the observed data points and the predicted ones by the RF model. This is evident from the small discrepancies visible in the line graph, indicating a close alignment between the actual and expected data.

7.3 Extreme Gradient Boost

Fig 14 (a) and (b) present a comparison of the predicted and observed outcomes generated by the XGB model. The RF model's predictions on both the training and test data sets were surpassed by the XGB model's implementation (R^2 = 0.935 and R^2 = 0.845, respectively).

The better accuracy observed in XGB compared to RF appears to be the result of gradient boosting. This technique combines the predictions of multiple decision trees sequentially, enabling it to capture intricate relationships in the data and improve accuracy. RF, on the other hand, builds multiple decision trees independently and averages their predictions, which can be more successful for certain complex datasets.

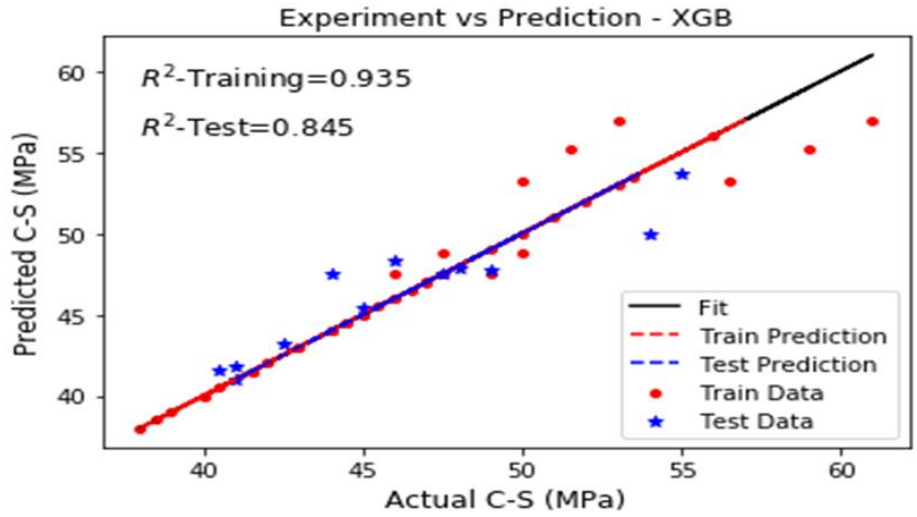

(a)

(b)

Fig. 14. (a) Correlation between the actual and predicted XGB model results and (b) Error graph- XGB

7.4 Gradient Boost

Fig 15 (a) and (b) provide an analysis in comparison to the observed and anticipated outputs of the GB model. Fig 15 (a) presents the correlation between the experimental outcomes and the predictions derived by the GB model. The GB model has been put into action successfully with an impressive 0.934 R^2 score on the training data and a commendable 0.929 on the test dataset. The outcome of the GB model demonstrates a higher level of precision compared to the outputs of the RF and XGB models.

The error graph- GB demonstrates a strong correspondence between the observed data points and the anticipated data points, as evidenced by the low discrepancy observed in the line graph. The GB model has demonstrated superior accuracy in comparison to alternative models, with the fewest errors. The reasons for achieving the highest accuracy in the GB model are because of the model's mechanism, such as randomness and ensemble diversity, which can greatly contribute to improved performance.

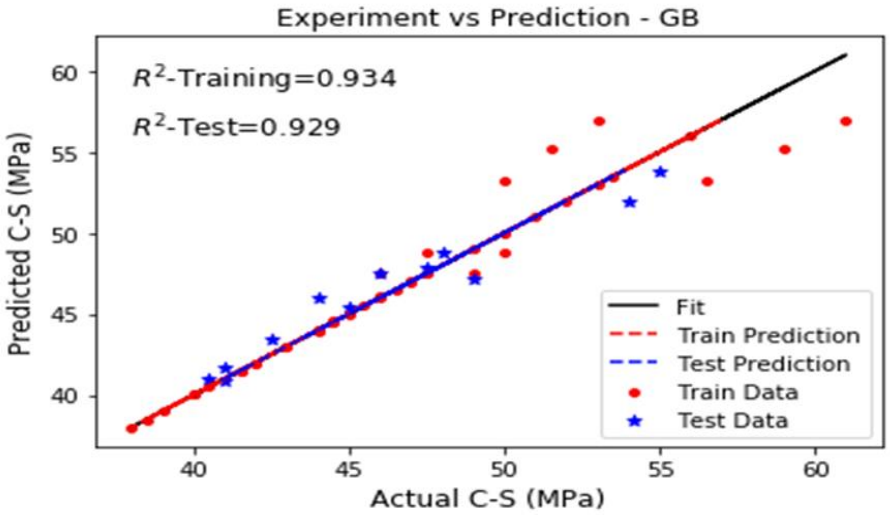

(a)

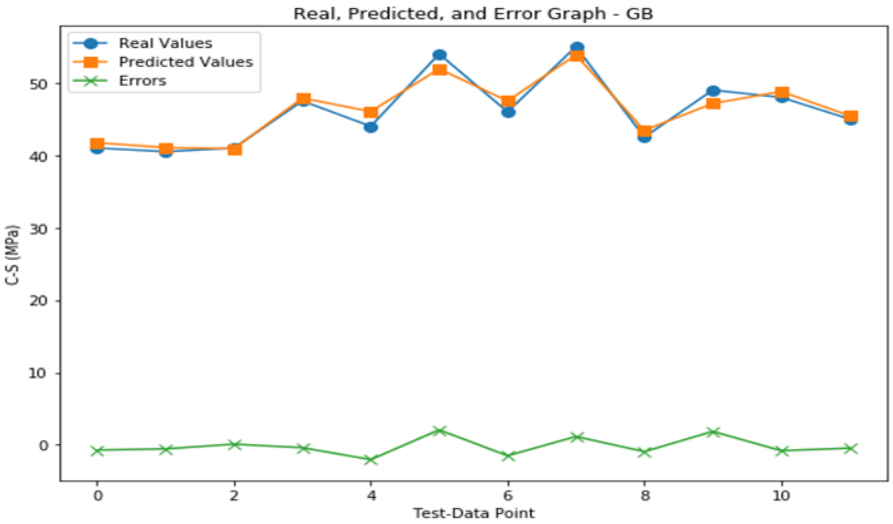

(b)

Fig 15(a): Correlation between the actual and predicted GB model results and (b) Error graph- GB

Firstly, the outcome of this randomness has the potential to various accuracy scores when the models are trained multiple times. However, this presents an opportunity for improvement and discovering even better results. If the GB model's random initialization aligns favorably, it has the potential to produce even better accuracy. Secondly, the GB model offers the exciting opportunity to combine with a diverse set of base models, such as decision trees with different characteristics or other learners, to form a powerful ensemble. If the GB ensemble is well-designed, it has the potential to outperform XGB.

8. Conclusion

- Workability parameters such as slump flow and L-Box values exhibited a decrease as molarity increased due to the higher solute concentration leading to stronger intermolecular forces, reducing flowability and causing slower movement through the funnel, while V-funnel values demonstrated an increase So, as molarity increases, the activator solution will be thicker and moves more slowly, which will cause higher V-funnel values. The values were marginally greater than the specified limits of EFNARC at 10M and 12M for only the 30% replacement of GGBS with metakaolin.

- The slump flow decreases by 3.6% to 4.3%, 2.9% to 5.1%, and 1.5% to 3.7% with 10% and 30% metakaolin replacement for 8M, 10M, and 12M, while the V-funnel flow time rises by 5.5% to 19.26%, 9% to 22.72%, and 1.75% to 16.66%. The slump flow & V funnel values show low workability as metakaolin content increases. Similarly, the L-box test also shows a decline in the blocking ratio, decreasing by 4.50% to 7.86% with higher metakaolin and sodium hydroxide concentrations. This is due to metakaolin's higher pozzolanic nature leading to higher water demand.
- The percentage increase in strength from 8M to 10M and from 10M to 12M at the end of 90days was 11.57% and 15.09% for the M1 series, 5.37% and 14.28% for the M2 series, 3.23% and 14.89% for the M3 series, and 9.87% and 14.60% for the M4 series. The compression strength is enhanced with increasing molarity, irrespective of the mixture. As the molarity increases the strength of SCGC increases due to the higher concentration of sodium hydroxide solution leading to higher alumina-silicate gel and densified matrix in the mix employed. The same trend is observed in the split tensile, flexural, and shear strength of concrete. Irrespective of molarity, all mixtures, including the reference mix, the shear strength exceeded 2.5MPa.
- Irrespective of the binder proportions and molarities, GGBS/Metakaolin-based oven-cured SCGC generally gains strength with age. The GGBS and Metakaolin-based SCGC produce a three-dimensional aluminosilicate network that binds the particles together, which gives a higher strength gain in the mixes developed with respect to age, type of curing, and age of curing.
- The compressive strength of SCGC exhibited a decrease across all ages as the volume of metakaolin added to GGBS increased from 0% to 30% due to metakaolin appearing more compact, uniform, and homogeneous, with fewer unreacted particles & has experienced partial alkali activation.
- An increase in molarity and the passage of time both result in a more compact matrix and fewer micro-cracks in GGBS composites, which translates to greater strength. However, when metakaolin was used in place of GGBS, more water was needed to achieve flow; this led to a rise in unreacted CSH crystals, microscopic gaps, and micro-cracks, resulting in a less compact structure and a decrease in strength.
- As the percentage of metakaolin in the material increased, the impact resistance decreased, and vice versa for GGBS. Energy absorption by SCGC increased with increasing molarity, and 10% metakaolin substitution of GGBS resulted in the highest energy absorption capacity across all test days. The denser microstructure formed by metakaolin can reduce the material's ability to absorb energy upon impact. Additionally, metakaolin's higher silica content can increase the overall brittleness of the geopolymer concrete, limiting its capacity for deformation under impact loading.
- The gradient boost model exhibited superior performance due to its superior accuracy, regularization, and ability to handle noisy data, making it ideal for optimizing mixes in terms of mechanical properties compared to other machine learning models on the test dataset, achieving an R^2 of 0.929, MAE of 0.593, RMSE of 1.361, and MSE of 1.852 when predicting the compressive strength of GGBS.
- R^2 training, R^2 test, MAE, MSE, and RMSE are helpful for assessing the model's accuracy, error distribution, and ability to generalize, providing a comprehensive understanding of model performances.
- The successful implementation of machine learning models has delivered impressive results in accurately predicting compressive strength on our experimental dataset. These models show great potential for applications in fields like construction and materials science, with promising predictive accuracies.
- The results demonstrate that machine learning models with hyperparameter tuning are highly effective in achieving enhanced prediction accuracy even on small datasets.

9. Future Scope of The Present Research

- The study can be extended further by employing natural fibers in self-compacting geopolymer concrete.

- This study can be extended to know the effect of temperature of SCGC with varying temperatures (elevated temperature study)
- A durability study can be employed for the above mixes to study the effect of early and long-term acid/salt exposure.
- Further, the sustainability analysis can be conducted for the above mix proportions.
- Cost analysis of Self-compacting geopolymer concrete can be studied.

References

[1] Md Khalid S, Shobha MS. Ternary blended geopolymer concrete: a review. In: IOP Conference Series: Earth and Environmental Science. 2021;822:1-8. https://doi.org/10.1088/1755-1315/822/1/012043

[2] Khalid SM, Shobha MS. Effect of ternary blends on mechanical strength, durability and microstructural properties of geopolymer concrete. Iran J Sci Technol Trans Civ Eng. 2023. https://doi.org/10.1007/s40996-023-01241-4

[3] HM T, Unnikrishnan S. Utilization of industrial and agricultural waste materials for the development of geopolymer concrete: a review. Mater Today Proc. 2022;65:1290-1297. https://doi.org/10.1016/j.matpr.2022.04.192

[4] Khalid S, Reshma T, Shobha M, Priyanka G, Siriki VS. Analysis of strength and durability properties of ternary blended geopolymer concrete. Mater Today Proc. 2021;54:259-263. https://doi.org/10.1016/j.matpr.2021.08.307

[5] Zhang Z, Yao X, Huajun Z, Yue C. Role of water in the synthesis of calcined kaolin-based geopolymer. Appl Clay Sci. 2009;43:218-223. https://doi.org/10.1016/j.clay.2008.09.003

[6] Kamseu E, Rizzuti A, Leonelli C, Perera D. Enhanced thermal stability in K2O-metakaolin-based geopolymer concretes by Al2O3 and SiO2 fillers addition. J Mater Sci. 2010;45(7):1715-1724. https://doi.org/10.1007/s10853-009-4108-1

[7] Fang Y, Li H, Wang Z, Zhang K, Cui P, Dong B. The effect of metakaolin on the hardening process of alkali-activated slag by using electrochemical impedance spectroscopy. Earth Environ Sci. 2019. https://doi.org/10.1088/1755-1315/300/5/052011

[8] Justice JM, Kennison LH, Mohr BJ, Beckwith SL, McCormick LE, Wiggins B, et al. Comparison of two metakaolins and a silica fume used as supplementary cementitious materials. In: Proceedings of the Seventh International Symposium on Utilization of High-Strength/High-Performance Concrete, ACI SP-228. Washington DC: American Concrete Institute; 2005. p. 213-226.

[9] Phair JW, van Deventer JSJ, Smith JD. Effect of Al source and alkali activation on Pb and Cu immobilization in fly-ash based 'geopolymers'. Appl Geochem. 2004;19(3):423-434. https://doi.org/10.1016/S0883-2927(03)00151-3

[10] Malhotra VM, Mehta PK. High-performance, high-volume fly ash concrete: materials, mixture proportioning, properties, construction practice, and case histories. Aug 2002.

[11] HM T, Unnikrishnan S. Mechanical strength and microstructure of GGBS-SCBA based geopolymer concrete. J Mater Res Technol. 2024;7816-7831. https://doi.org/10.1016/j.jmrt.2023.05.051

[12] Kong DLY, Sanjayan JG, Sagoe-Crentsil K. Comparative performance of geopolymers made with metakaolin and fly ash after exposure to elevated temperatures. Cem Concr Res. 2007;37(12):1583-1589. https://doi.org/10.1016/j.cemconres.2007.08.021

[13] Siddique R. Utilization of industrial by-products in concrete. Procedia Eng. 2014;95:335-347. https://doi.org/10.1016/j.proeng.2014.12.192

[14] Shen J, et al. Prediction of compressive strength of alkali-activated construction demolition waste geopolymers using ensemble machine learning. Constr Build Mater. 2022;360:129600. https://doi.org/10.1016/j.conbuildmat.2022.129600

[15]IS 383 (1970): Specification for coarse and fine aggregates from natural sources for concrete, Bureau of Indian Standards, Manak Bhavan, 9, Bhadur Shah Zafar Marg, New Delhi, 110002.

[16] EFNARC Guidelines for SCC. Available from: https://wwwp.feb.unesp.br/pbastos/c.especiais/Efnarc.pdf.

[17]IS 516 (1959): Method of tests for strength of concrete, Bureau of Indian Standards, Manak Bhavan, 9, Bhadur Shah Zafar Marg, New Delhi, 110002.

[18] Bairagi NK, Modhera CD. Shear strength of fiber-reinforced concrete. ICI J. 2001;47-53.

[19] Baruah P, Talukdar S. A comparative study of compressive, flexural, tensile and shear strength of concrete with fibers of different origins. 2007;81:17-24.

[20]IS-456 (2000), Plain and Reinforced Concrete—Code of Practice, Bureau of Indian Standards, Manak Bhavan, 9, Bhadur Shah Zafar Marg, New Delhi, 110002.

[21] ACI PRC-544.4-18: Guide to design with fiber-reinforced concrete. Sep 29, 2023. Available from: https://www.concrete.org/store/productdetail.aspx?ItemID=544418&Language=English&Units=US_AND_METRIC.

[22] Demie S, Nuruddin MF, Shafiq N. Effects of micro-structure characteristics of interfacial transition zone on the compressive strength of self-compacting geopolymer concrete. Constr Build Mater. 2013;41:91-98. https://doi.org/10.1016/j.conbuildmat.2012.11.067
[23] Hulipalled P, Algur V, Lokesha V, Saumya S, Satyanarayan. Interpretable ensemble machine learning framework to predict wear rate of modified ZA-27 alloy. Tribol Int. 2023;188:108783. https://doi.org/10.1016/j.triboint.2023.108783
[24] Hulipalled P, Algur V, Veera L, Saumya S. Intelligent retrieval of wear rate prediction for hypereutectoid steel. Multiscale Multidiscip Model Exp Des. 2023;6:1-13. https://doi.org/10.1007/s41939-023-00172-x
[25] Hulipalled P, Algur V, Veera L. An approach of data science for the prediction of wear behaviour of hypereutectoid steel. J Bio Tribo Corros. 2022;8. https://doi.org/10.1007/s40735-022-00668-y
[26] Algur V, Hulipalled P, Veera L, Nagaral M, Auradi V. Machine learning algorithms to predict wear behavior of modified ZA-27 alloy under varying operating parameters. J Bio Tribo Corros. 2022;8. https://doi.org/10.1007/s40735-021-00610-8
[27] Sumanth Kumar B, Sen A, Rama SD. Shear strength sustainable construction materials. Select Proceedings of ASCM 2019. 2019;68:105-117. https://doi.org/10.1007/978-981-15-3361-7_8
[28] Wang Q, Ahmad W, Ahmad A, Aslam F, Mohamed A, Vatin NI. Application of soft computing techniques to predict the strength of geopolymer composites. Polymers. 2022;14:1074. https://doi.org/10.3390/polym14061074